Thermal Sensing Using Micro-ring Resonators in Optical Network-on-Chip

Weichen Liu[1], Mengquan Li[2], Wanli Chang[3], Chunhua Xiao[2], Yiyuan Xie[4], Nan Guan[5], Lei Jiang[6]

[1]School of Computer Science and Engineering, Nanyang Technological University, Singapore
[2]College of Computer Science, Chongqing University, China
[3]Department of Computer Science, University of York, UK
[4]College of Electronic and Information Engineering, Southwest University, China
[5]Department of Computing, Hong Kong Polytechnic University, Hong Kong
[6]School of Informatics, Computing and Engineering, Indiana University Bloomington, USA

Abstract—In this paper, we for the first time utilize the micro-ring resonators (MRs) in optical networks-on-chip (ONoCs) to implement thermal sensing without requiring additional hardware or chip area. The challenges in accuracy and reliability that arise from fabrication-induced process variations (PVs) and device-level wavelength tuning mechanism are resolved. We quantitatively model the intrinsic thermal sensitivity of MRs with fine-grained consideration of wavelength tuning mechanism. Based on it, a novel PV-tolerant thermal sensor design is proposed. By exploiting the hidden 'redundancy' in wavelength division multiplexing (WDM) technique, our sensor achieves accurate and efficient temperature measurement with the capability of PV tolerance. Evaluation results based on professional photonic component and circuit simulations show an average of 86.49% improvement in measurement accuracy compared to the state-of-the-art on-chip thermal sensing approach using MRs. Our thermal sensor achieves stable performance in the ONoCs employing dense WDM with an inaccuracy of only 0.8650 K.

I. INTRODUCTION

Continuous technology scaling in manycore processors leads to severe overheating issues. To achieve effective on-chip temperature management, an accurate yet efficient thermal sensing solution is critical. CMOS-compatible electric sensors [1]–[3] are the popular ways of obtaining runtime temperature information required for dynamic thermal management. They possess high accuracy and efficiency but introduce additional overheads on hardware and chip area.

Optical network-on-chip (ONoC) [4], as an emerging communication architecture, offers ultrahigh bandwidth, low latency and low power dissipation for new-generation manycore systems, especially employing wavelength division multiplexing (WDM) technology. Micro-ring resonators (MRs) are versatile components in ONoCs. As shown in Fig. 1(a), a MR consist of one ring and two straight waveguides. When a MR is configured to be switched *off*, the optical signals from the *Input* port will be delivered to the *Through* port. Otherwise, the optical signal whose wavelength is within the resonant wavelength range gets resonated into the ring and delivered to the *Drop* port, while the signals whose wavelength are beyond the range is filtered. The wavelength selectivity of MR lends itself naturally for WDM operation. Cascaded MRs have been widely used as basic optical filtering element (BOFE) (Fig. 1(b)) at the receiver side to demultiplex the WDM wavelengths before optical signals reaching the photodetectors (PDs).
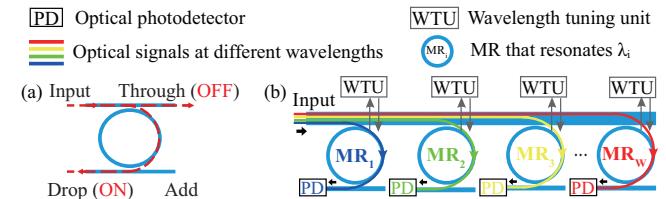

Fig. 1: (a) Micro-ring resonator (MR); (b) Basic optical filtering element (BOFE).

MRs are highly sensitive to temperature variations (TVs). The resonant wavelength of a MR red-shifts with increasing temperatures and blue-shifts with decreasing ones. Due to TVs, the undesired mismatch between the signal wavelength and the resonant wavelength of the MR will result in additional optical power loss. The intrinsic thermal sensitivity of MRs in ONoCs renders them an attractive choice for on-chip temperature sensing. Compared to traditional electric sensors, MR-based optical thermal sensors have favorable properties of compact size, immunity to electromagnetic interference and robustness against mechanical shock [5]. What's more, the well-modeled temperature dependence of MRs [6] (i.e., the relationship between the resonant wavelength, as well as the optical power loss, of a MR and its ambient temperature) make them practical.

However, fabrication-induced process variations (PVs), as well as the device-level wavelength tuning mechanism [7], complicate this problem. PV in photolithography affects the cross-section, the width and height, of etched silicon channels, resulting in significant wavelength drifts for MRs (termed PV-drifts for short and TV-drifts denote the resonant wavelength shifts due to TVs). Recent laboratory measurements have reported a standard deviation of 1.3 nm chip-scale width variation, which translates to a 0.76 nm resonant wavelength shift (i.e., equivalent to the TV-drifts under a temperature variation of 12.7 K) [8]. For most MR-based temperature sensors that operate by monitoring the resonant wavelength

shifts, PVs greatly decrease their accuracy for temperature measurement because the PV-drifts may be mistaken for TV-drifts. So does the device-level wavelength tuning technique, which will compensate for the wavelength shifts of MRs due to PVs and TVs simultaneously. For reliable data transmission, local wavelength tuning is generally applied for every MR in ONoCs [9]. Through heating or current injection, it potentially achieves wavelength-locking and stabilization [10]. These two factors have been overlooked in the demonstrated results of existing MR-based thermal sensors but must be considered for accurate sensor designs.

In this paper, we for the first time utilize MRs to implement on-chip thermal sensing without requiring extra hardware or chip area, and further resolve the challenges in accuracy and reliability that arise from PVs and local wavelength tuning. Our contributions are summarized as follows.

- We quantitatively model the intrinsic thermal sensitivity of MRs with fine-grained consideration of the impact of wavelength tuning mechanism.
- A PV-tolerant thermal sensor design is further proposed. By exploiting the hidden 'redundancy' in WDM technique, it achieves accurate and efficient temperature measurement with the capability of PV tolerance.
- Evaluation results based on professional photonic component and circuit simulations show that the average prediction error of our thermal sensitivity model is 0.5521 K and achieves 79.5% prediction improvement than the state-of-the-art temperature model. Under PVs, the PV-tolerant thermal sensor averagely improves the measurement accuracy by 86.49% compared to the most advanced on-chip thermal sensing approach using MRs. It achieves stable performance in the ONoCs employing dense WDM (DWDM) with an inaccuracy of only 0.8650 K.

II. THERMAL SENSITIVITY OF MR WITH CONSIDERATION OF DEVICE-LEVEL WAVELENGTH TUNING

A linear relationship between the resonant wavelength shift and TVs is widely recognized for MRs. Given the nominal resonant wavelength, λ_0, at the default temperature (typically room temperature), T_0, the formula of the resonant wavelength of a MR, λ_{MR}, and the ambient temperature, T_{MR}, can be expressed as follow:

$$\lambda_{MR} = \lambda_0 + \rho \cdot (T_{MR} - T_0) \qquad (1)$$

where ρ is the temperature-dependent resonant wavelength shift coefficient of the MR and is about 0.06 nm/K at the 1,550 nm wavelength range [9].

The undesired deviation from the peak resonant wavelength caused by TVs will result in additional power loss. According to the traveling wave theory [6], the optical power loss of a MR due to TV, L_{MR}^t, can be formulated as follow:

$$L_{MR}^t = 10log\left(\left(\frac{2\kappa^2 + \kappa_p^2}{2\kappa^2}\right)^2\left(1 + \frac{4(\lambda_{TX} - \lambda_0 - \rho(T_{MR} - T_0))^2}{\theta^2}\right)\right) \qquad (2)$$

where κ^2 is the fraction of optical power coupling between the waveguides and the ring. κ_p^2 is the fraction of intrinsic power losses per round-trip in the ring. λ_{TX} is the wavelength of

the incident optical signal, which typically equals the nominal resonant wavelength of the MR (i.e., $\lambda_{TX} = \lambda_0$). θ is the -3dB bandwidth of the drop-port power transfer spectrum.

The formula (1) and (2) well model the temperature dependence of MRs, which make it possible to utilize single MR for on-chip thermal sensing. However, to implement high-performance and reliable ONoCs, device-level wavelength tuning is widely employed for MRs to compensate for their wavelength shifts. Altering the free-carrier concentration in a MR core or tuning the local temperature of the MR based on an integrated microheater, the resonant wavelength of the MR shifts towards the blue or red end of the spectrum, respectively. Wavelength tuning technique achieves a stable locking of MR resonances at the expense of extra power consumption. The regulation power consumed for a MR can be formulated as:

$$P_{tuning} = \epsilon \cdot (\lambda_{MR} - \lambda_0) \qquad (3)$$

where ϵ is the tuning efficiency in mW/nm; $\lambda_{MR} - \lambda_0$ denotes the tuning distance, $\Delta\lambda_{tuning}$.

As the resonant wavelength of a MR is realigned with the nominal wavelength through local tuning, the optical power loss of the MR caused by the undesired TV-drifts would be largely reduced. According to Eq. (2) and (3), the power loss reduced by wavelength tuning can be expressed as follow:

$$L_{tuning} = 10log\left(\left(\frac{2\kappa^2 + \kappa_p^2}{2\kappa^2}\right)^2\left(1 + \frac{4P_{tuning}^2}{\epsilon^2\theta^2}\right)\right) \qquad (4)$$
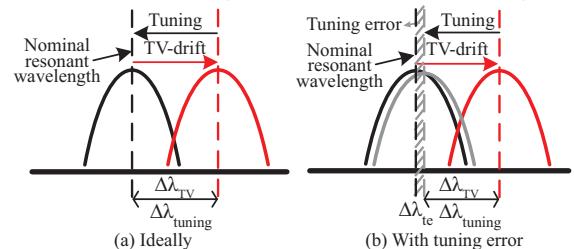
Fig. 2: Effect of device-level wavelength tuning on MRs.

We illustrate the scenario where a MR employs local wavelength tuning in Fig. 2. Ideally, the tuning distance equals the TV-drift ($\Delta\lambda_{tuning} = \Delta\lambda_{TV}$) and the total power loss of a MR is zero. Given the power consumed by wavelength tuning, P_{tuning}, we can easily obtain the ambient temperature of the MR as $T_{MR} = T_0 + P_{tuning}/(\epsilon \cdot \rho)$. Nevertheless, wavelength tuning mechanism is not perfectly mature. The resonant wavelength of the MR after tuning is probably aligned not to the nominal wavelength (ideal value), but to a wavelength around the ideal one with a tuning error ($\Delta\lambda_{te}$ in Fig. 2(b)); consequently, a small amount of power loss is caused. According to the law of energy conservation, for a MR under TVs, the power loss before tuning, L_{MR}^t, is the sum of the power loss after tuning and the power loss compensated by local wavelength tuning. It can be formulated as follow:

$$L_{MR}^t = P_{TX}^o - P_{RX}^o + L_{tuning} \qquad (5)$$

where P_{TX}^o is the optical power of the incident optical signal, which is typically known in ONoCs. P_{RX}^o is the optical power received by the PD at the receiver side. $P_{TX}^o - P_{RX}^o$ denotes the total power loss of the MR after tuning (i.e., the loss resulted from the tuning error).

We formulate the thermal sensitivity of MRs with fine-grained consideration of local wavelength tuning as Eq. (6), which describes the relationship between the tuning power (P_{tuning}), the power loss of a MR after tuning ($P_{TX}^o - P_{RX}^o$), and its ambient temperature (T_{MR}).

$$\boldsymbol{T_{MR}} = T_0 + \frac{\sqrt{\left(\frac{\theta^2}{4} + \frac{P_{tuning}^2}{\epsilon^2}\right) \cdot 10^{\left(\frac{P_{TX}^o - P_{RX}^o}{10}\right)} - \frac{\theta^2}{4}} + (\lambda_{TX} - \lambda_0)}{\rho}$$
(6)

With the single-wavelength incident signal whose wavelength equals to the nominal resonant wavelength of a MR, Eq. (6) can be simplified to $T_{MR} = T_0 + f(P_{RX}^o, P_{tuning})$ where the other parameters are constant for the MR. The temperature of the MR can be obtained once we know the measured optical power received by the PD and the power consumed by wavelength tuning, which are both easily known in ONoCs. This physical model functions as the theoretical foundation of this paper. By analyzing the impact of device-level wavelength tuning on the thermal sensitivity of MRs, which has been overlooked in the state-of-the-art temperature dependence model [6], our model enhances the measurement accuracy and reliability of MR-based thermal sensor designs.

III. PV-TOLERANT THERMAL SENSOR

Nevertheless, PVs compound this problem. Under PVs, wavelength tuning technique is able to correct PV-drifts and TV-drifts simultaneously. As the power loss caused by PV-drifts is mistaken for that caused by TV-drifts, an inaccurate monitoring temperature will be derived from Eq. (6). Therefore, it is critical to remove the impact of PVs for accurate temperature prediction.

A common solution for correcting PV-drifts is post-fabrication calibration at the device level, which determines the fabric error through variation characterization during chip testing and then calibrate it carefully for every MR. No additional power is required after successful calibration. However, this technique is immature and less commercially practical [11], [12]. Firstly, it is difficult to do post-fabrication calibration for ONoCs where thousands and millions of MRs exist. Every MR differs from one another and requires precise control. Secondly, the method of trimming the cladding material to implement calibration is unstable currently. Lastly, the technique would decrease the quality factor of MRs, threatening their reliability. Current solutions for PV mitigation introduce huge overhead and lack scalability.

In this work, we implement PV-tolerant thermal sensing by exploiting the 'redundancy' in WDM technique at the system level. By concurrently transmitting multiple optical signals at different wavelengths on a single waveguide, WDM dramatically increases network bandwidth. BOFE has been widely used at the optical receiver to demultiplex the WDM wavelengths in WDM-based ONoCs. The cascaded MRs in a BOSE filter out their own resonant wavelengths, which can be regarded as the duplication of the filtering operation using a single MR. The hidden 'redundancy' in WDM can be utilized for PV tolerance.

The PV-drift of every MR is determined by its physical dimensions. If we implement temperature sensing based on a specific MR, a constant measurement error results from the static PV-drift of the MR. In contrast, the PV-drifts of the multiple MRs in a BOFE are random due to the fabrication non-uniformity, which will result in various temperature measurement errors when employing them as sensors separately. These temperature errors caused by PVs may potentially cancel each other out with an average value of zero. Taking a four-wavelength BOFE comprising four MR-based add-drop filters as an example, the ambient temperature of the four MRs is identical due to the compact structure and small footprint of BOFEs. When employing these MRs for thermal sensing separately, we assume that the temperature errors caused by PVs are +1 K, -3 K, +4 K, and -2 K, with an average error of zero. The impact of PVs on measurement accuracy can be counteracted if we use their average temperature as the measured temperature.
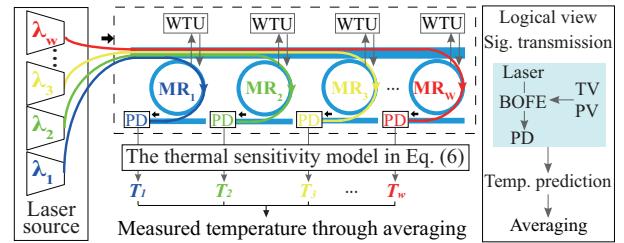
Fig. 3: The PV-tolerant thermal sensor design.

As shown in Fig. 3, we propose a PV-tolerant thermal sensor design. The sensor is comprised of a multi-wavelength laser source, a BOFE and PDs, which are all readily available in typical WDM-based ONoCs. The laser source can be implemented by an array of VSCELs [13], in which optical signals can be modulated directly by the driving current without modulators. The MRs in the BOFE filter out their own designated resonant wavelengths from the input wavelengths, demultiplexing the W wavelengths before the optical signals reaching the PDs. For every single MR, based on the known input optical power emitted from the laser, the received optical power measured by the PD and the power consumed by the corresponding wavelength tuning unit (WTU), we can derive a predicted temperature from Eq. (6) (e.g., T_1, T_2, ..., T_w in Fig. 3). Using the average value of the predicted temperatures as the measured temperature, we can achieve accurate yet efficient temperature measurement with the ability to PV tolerating.

IV. EVALUATION

A. Accuracy of the thermal sensitivity model

We use a compact silicon-on-insulator (SOI) MR with a radius of 5 μm to experimentally verify the accuracy of our thermal sensitivity model. The coupling gaps between the silicon waveguides and ring are 100 nm with a cross-section of 400 nm × 180 nm. We simulate the MR and study its optical characteristics through component-level FDTD simulations [14]. The wavelength tuning mechanism applied for the MR is studied through circuit-level INTERCONNECT

simulations [15]. The frequency responses of the MR obtained from FDTD simulations would be directly exported into INTERCONNECT, in which the optical characteristics of the MR under local wavelength tuning can be analyzed through optical analyzer. According to the simulation results, the wavelength tuning mechanism applied in our experiments has a tuning efficiency of about 0.1692 nm/mW.
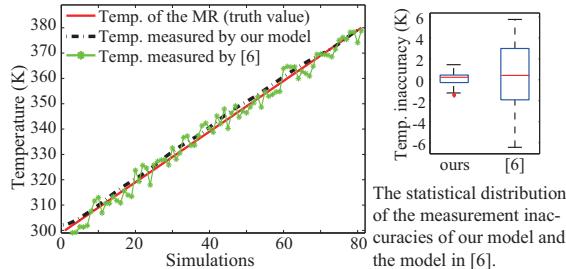

Fig. 4: Accuracy of our thermal sensitivity model.

Setting the incident light as the fundamental TE mode for wavelength at ∼1550 nm, with which the MR resonates at room temperature, we compare our thermal sensitivity model with the state-of-the-art thermal model presented in [6] for accuracy verification on temperature prediction. Work [6] formally models the thermo-optic effect of MRs without considering the impact of wavelength tuning technique. We conduct 80 groups of experiments, in which the temperature of the MR increases from 300 K to 380 K. The temperature of 380 K is an extremely high value for a silicon chip. As shown in Fig. 4, with fine-grained consideration of the effect of tuning mechanism on wavelength locking, our thermal sensitivity model has high prediction precision with an average difference of only 0.5521 K compared to the temperature of the MR (the ground truth value), and on average 79.5% of prediction improvement is achieved than the model in [6]. We further present a box-and-whisker diagram to display the statistical distribution of their temperature inaccuracies at the right side of Fig. 4. This accurate model provides a good foundation to our thermal sensor design.

B. Effectiveness of the PV-tolerant thermal sensor

We conduct 20 groups of experiments based on an eight-wavelength BOFE. The PVs of the MRs are characterized by using Normal distribution with a standard deviation of 1.3 nm in waveguide width, similar to the models in [8], [11]. We assume that the ambient temperature of the cascaded MRs is identical due to the compact structure and small footprint of BOFEs. In every group of experiment, the waveguide widths of the eight MRs are randomly generated and follow Normal distribution, $N(400, 1.3^2)$. Given a random ambient temperature within the range from 300 K to 380 K, the optical characteristics of the eight MRs are obtained from FDTD simulations, which are then exported into INTERCONNECT for implementing wavelength tuning. Based on the simulation results and the thermal sensitivity model in Eq. (6), we can obtain the measured temperature of our PV-tolerant sensor.

As shown in Fig. 5(a), the black dots and blue circles are the measurement errors obtained by sensing with every single MR in the BOFE, based on our thermal sensitivity model in Eq. (6) and the state-of-the-art thermal model in [6], respectively, and the red curve is the temperature inaccuracy obtained by our PV-tolerant sensor. The predicted temperature obtained by single MR varies with an error of up to > 20 K under PVs. Compared to the sensor implementing thermal sensing with single MR, our thermal sensor can largely reduce the measurement error by 81.3% on average in virtue of the capability of PV tolerance. By integrating with the accurate thermal model in Eq. (6), the inaccuracy of our thermal sensor is only 0.8650 K on average, improving the measurement accuracy by 86.49% compared to the single-MR sensor using the state-of-the-art thermal model in [6]. Furthermore, similar experiments are conducted based on the BOFEs with different number of MRs (ranging from 8 to 16). The average absolute errors of the thermal sensors based on different size of BOFEs are illustrate in Fig. 5(b). It can be observed that our sensor achieves stable performance in the ONoCs employing DWDM with an average of 82.47% accuracy improvement.
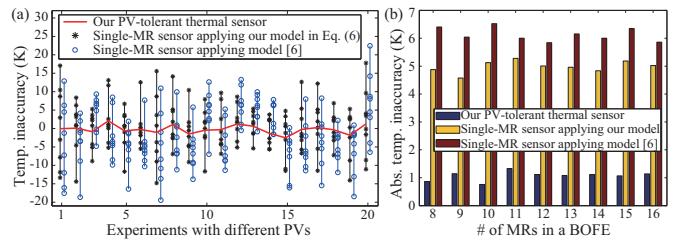

Fig. 5: Effectiveness of our PV-tolerant thermal sensor. (a) Accuracy comparison between our thermal sensor and the sensors based on single MR applying our model in Eq. (6) and the state-of-the-art thermal model in [6]; (b) Our sensor achieves stable performance in the ONoCs employing DWDM.

REFERENCES

[1] K. Makinwa, "Smart temperature sensors in standard cmos," *Procedia Engineering*, vol. 5, pp. 930–939, 2010.
[2] T. Anand, K. A. Makinwa, and P. K. Hanumolu, "A VCO based highly digital temperature sensor with 0.034°c/mv supply sensitivity," *IEEE Journal of Solid-State Circuits*, vol. 51, no. 11, pp. 2651–2663, 2016.
[3] U. Sönmez, F. Sebastiano, and K. A. Makinwa, "11.4 1650 μm^2 thermal-diffusivity sensors with inaccuracies down to ±0.75°c in 40nm cmos," in *ISSCC*. IEEE, 2016, pp. 206–207.
[4] K. Bergman, L. P. Carloni, A. Biberman, J. Chan, and G. Hendry, *Photonic network-on-chip design*. Springer, 2014.
[5] H. T. Kim and M. Yu, "Cascaded ring resonator-based temperature sensor with simultaneously enhanced sensitivity and range." *Optics Express*, vol. 24, no. 9, p. 9501, 2016.
[6] W. Liu, P. Wang, M. Li, Y. Xie, and N. Guan, "Quantitative modeling of thermo-optic effects in optical networks-on-chip," in *GLSVLSI*, 2017, pp. 263–268.
[7] K. Padmaraju and K. Bergman, "Resolving the thermal challenges for silicon microring resonator devices," *Nanophotonics*, vol. 3, no. 4-5, pp. 269–281, 2014.
[8] Z. Li, *et al*, "Reliability modeling and management of nanophotonic on-chip networks," *IEEE TVLSI*, vol. 20, no. 1, pp. 98–111, 2012.
[9] Y. Ye, *et al*, "System-level modeling and analysis of thermal effects in wdm-based optical networks-on-chip," *IEEE TCAD*, vol. 33, no. 11, pp. 1718–1731, 2014.
[10] C. Nitta, M. Farrens, and V. Akella, "Addressing system-level trimming issues in on-chip nanophotonic networks," in *HPCA*. IEEE, 2011, pp. 122–131.
[11] Y. Xu, J. Yang, and R. Melhem, "Tolerating process variations in nanophotonic on-chip networks," in *ISCA*, 2012, pp. 142–152.
[12] N. Boynton, *et al*, "Characterization of systematic process variation in a silicon photonic platform," in *OI*. IEEE, 2017, pp. 11–12.
[13] A. Syrbu, A. Mereuta, V. Iakovlev, A. Caliman, P. Royo, and E. Kapon, "10 gbps VCSELs with high single mode output in 1310nm and 1550 nm wavelength bands," in *OFC/NFOEC*. IEEE, 2008, pp. 1–3.
[14] "Lumerical FDTD Solutions," https://www.lumerical.com/tcad-products/fdtd/.
[15] "Lumerical INTERCONNECT (PIC Simulation)," https://www.lumerical.com/tcad-products/interconnect/.